INTERNATIONAL JOURNAL FOR NUMERICAL METHODS IN FLUIDS, VOL. 14, 109–124 (1992)

A COMPARISON OF SPATIAL GRIDS FOR NUMERICAL MODELLING OF FLOWS IN NEAR-COASTAL SEAS

R. W. LARDNER AND Y. SONG

Mathematics Department, Simon Fraser University, Burnaby, British Columbia, V5A 1S6, Canada

SUMMARY

Three-dimensional algorithms for the numerical computation of flows caused by tides or meteorological forcing are developed for four of Arakawa's spatial grid types using a spectral method in the vertical dimension. Three of the grids, in which the velocity components are computed at the same grid points, offer potential advantages over the commonly used C-grid. The computed results from the four grids are compared for three test problems based on the linearized hydrodynamical equations. It is concluded that the B-grid provides a viable alternative to the C-grid, with significant advantages when a spectral method is used.

KEY WORDS Numerical tidal model Spectral method Arakawa grids

INTRODUCTION

Some of the computationally most efficient numerical algorithms for three-dimensional simulation of flows in coastal seas have been based on a spectral method for the vertical co-ordinate combined with finite differences in the horizontal directions.[1–7] Most of the finite difference schemes that have been developed for such hydrodynamical modelling have been based on an Arakawa C-grid, starting with the two-dimensional algorithms of Hansen, Leendertse and others[8–10] down to the more recent three-dimensional algorithms[11–14] and including the algorithms based on the spectral method.[1–7] While this choice of grid has the advantage of providing natural centred difference approximations to most of the dominant terms and of minimizing numerical dispersion,[15] it does lead to certain difficulties for some three-dimensional computations.

The first of these[6] is the occurrence of spurious numerical boundary layers unless the Coriolis terms are treated carefully. Since the two horizontal velocity components are computed at different spatial points with a C-grid, it is necessary to average the Coriolis terms in each momentum equation over the four neighbouring points at which the opposite velocity component is computed. Adjacent to a coast, one or more of these four points will actually lie on the coast, and the velocity components at such points are maintained at zero by the usual algorithms. The result is that the four-point average gives an incorrect value for the interior point, and this leads to spurious velocities near the coast.

This difficulty does not arise for two-dimensional models based on the depth-averaged equations, since it is correct within the model to set the depth-averaged velocity components equal to zero at coastal points. Within the approximations of the usual three dimensional models,

0271–2091/92/010109–16$08.00

Received November 1990
Revised March 1991

however, the velocity profile through the water column is not zero at a coast: the narrow coastal boundary layer in which the flow overturns, accommodating itself to the physical boundary condition of zero normal flow, is not contained within the usual model equations. It is worth noting that the problem does not arise for certain three-dimensional algorithms of the splitting type[13,14] in which the C-grid is used only for the depth-averaged equations, and the vertical profiles are computed for both velocity components at the same horizontal grid points.

It has been pointed out by Jamart and Ozer[6] that for algorithms using a spectral method this problem may be overcome by averaging the Coriolis terms only over the adjacent points that are interior to the water body (called the 'wet-points-only' method). While this method is successful, it has the disadvantage of reducing the order of the local truncation error at near-coastal points, and this may produce a serious loss of accuracy for a region with an intricate coastline and consequently a large proportion of near-coastal points.

A second and probably more serious disadvantage of the C-grid which arises for spectral methods is that it is necessary to use the same basis functions at all grid points if the four-point average for the Coriolis terms is to give reasonably simple modal equations. The most efficient choice for the basis functions is to use eddy viscosity eigenfunctions,[1,4,7] since the modal equations are then decoupled. These are independent of position only if the eddy viscosity function has the same vertical profile at all points, apart from an overall scaling factor, and this is a severe restriction for a water body with widely varying parameters such as depth or bottom roughness. If this condition on the eddy viscosity is not satisfied, the Coriolis terms couple the modal equations.

Because of these problems, it appears worthwhile to consider using an alternative spatial grid for which both horizontal velocity components are computed at the same grid points. Of the five grid types described by Arakawa and Lamb,[15] those labelled A, B and E (see Figure 1) satisfy this requirement, so will certainly be simple to use when the eddy viscosity has arbitrary spatial variation. Since the two velocity components are computed at the same point, an additional benefit is that the two momentum equations can be solved simultaneously rather than sequentially as is necessary for the C-grid. This allows explicit treatment of the Coriolis terms to be easily avoided.

The A-, B- and E-grids lead to numerical schemes for the shallow water equations that have worse numerical dispersion than does the C-grid, particularly at wavelengths shorter than four grid lengths. However, the hydrodynamical models with which we are concerned involve significant damping through eddy viscosity and bottom friction, and to the extent we have tested these alternative grids, this does appear to be sufficient that the anomalous dispersion at short wavelengths does not cause difficulties. Arakawa's D-grid has both disadvantages of poor dispersion properties and velocity components at different points, so we have not considered it.

In Sections 2 and 3 we write down the basic equations for the spectral method, using eddy viscosity eigenfunctions as basis functions, and develop the appropriate numerical schemes for the A-, B-, C- and E-grids. For the purpose of comparison of the different spatial grids, we have based the schemes on the linearized hydrodynamical equations. In Section 4 the different schemes are compared using three test problems.

2. NUMERICAL SCHEMES

2.1. Basic equations

We use x, y, z as Cartesian co-ordinates with the z-axis pointing vertically upwards and the xy-plane occupying the undisturbed position of the water surface. The following list summarizes

the rest of the notation to be used:

$h(x, y)$	water depth
$\zeta(x, y, t)$	surface elevation at time t
$u(x, y, z, t)$, $v(x, y, z, t)$	horizontal velocity components
$p(x, y, t)$, $q(x, y, t)$	depth-integrated volume transports
f	Coriolis parameter
N	vertical eddy viscosity
g	acceleration due to gravity
ρ	fluid density
κ	coefficient of bottom friction
τ_x, τ_y	components of shear stress on the free surface.

The depth-integrated continuity equation takes the form

$$\frac{\partial \zeta}{\partial t}+\frac{\partial p}{\partial x}+\frac{\partial q}{\partial y}=0, \tag{1}$$

where the volume transports are defined as

$$p=\int_{-h}^{0} u\,\mathrm{d}z, \qquad q=\int_{-h}^{0} v\,\mathrm{d}z. \tag{2}$$

In the horizontal momentum equations as applied to flows in coastal seas it is usual to neglect the terms involving horizontal shear stress, which are small, and in many cases the advective terms are also negligible. Assuming a homogeneous sea, neglecting also the direct influence of tide-generating forces and making the usual hydrostatic pressure approximation, these equations may be written as

$$\begin{aligned} \frac{\partial u}{\partial t}-fv&=-g\frac{\partial \zeta}{\partial x}+\frac{\partial}{\partial z}\left(N\frac{\partial u}{\partial z}\right), \\ \frac{\partial v}{\partial t}+fu&=-g\frac{\partial \zeta}{\partial y}+\frac{\partial}{\partial z}\left(N\frac{\partial v}{\partial z}\right). \end{aligned} \tag{3}$$

The boundary conditions on the free surface and bottom are taken to be

$$\begin{aligned} \rho N\frac{\partial u}{\partial z}&=\tau_x \quad \text{and} \quad \rho N\frac{\partial v}{\partial z}=\tau_y \qquad \text{on } z=0, \\ \rho N\frac{\partial u}{\partial z}&=\kappa\rho u \quad \text{and} \quad \rho N\frac{\partial v}{\partial z}=\kappa\rho v \qquad \text{on } z=-h, \end{aligned} \tag{4}$$

where a linear form for bottom stress has been assumed, with κ the coefficient of bottom friction. A no-slip condition on the bottom is obtained in the limiting case $\kappa \to \infty$.

As discussed by Hunter,[16] the use of the form (4) for bottom stress is applicable in certain physical situations, although in most applications it would be more appropriate to use a quadratic dependence of bottom stress on velocity. However, here we are not concerned with using the most widely applicable physical model but rather with comparing the accuracy of various numerical algorithms, and for this purpose the linearized equations (3) and (4) are adequate. The most serious criticism of the grids other than the C-grid concerns the inaccurate dispersion at short wavelengths, and if this were to cause problems, they would show up in the linearized model (1)–(4). (It is, however, worth mentioning that the B-grid algorithm described later has been

extended to include both the advective terms and quadratic bottom friction and has been found to give accurate results in test problems.)[17]

It is convenient to use a σ-co-ordinate, defined as usual by

$$\sigma = 1 + z/h, \qquad z = -h(1-\sigma).$$

The momentum equations and boundary conditions can then be combined in complex form as

$$\frac{\partial U}{\partial t} + \mathrm{i}fU - h^{-2}\frac{\partial}{\partial \sigma}\left(N\frac{\partial U}{\partial \sigma}\right) = -g\left(\frac{\partial \zeta}{\partial x} + \mathrm{i}\frac{\partial \zeta}{\partial y}\right), \tag{5}$$

$$N\frac{\partial U}{\partial \sigma} = hS \quad \text{on } \sigma = 1,$$

$$N\frac{\partial U}{\partial \sigma} - \kappa h U = 0 \quad \text{on } \sigma = 0, \tag{6}$$

where

$$U = u + \mathrm{i}v, \qquad S = \frac{\tau_x + \mathrm{i}\tau_y}{\rho}. \tag{7}$$

2.2. Eddy viscosity eigenexpansion

The fundamental idea of the spectral method[1-7] is to expand the velocity components in terms of some set of basis functions. As originally proposed by Heaps,[1,2] it is advantageous to use as these functions the eigenfunctions of the Sturm–Liouville problem

$$\frac{\partial}{\partial \sigma}\left(N(\sigma)\frac{\partial \phi}{\partial \sigma}\right) + \lambda^2 \phi = 0, \tag{8}$$

$$N\frac{\partial \phi}{\partial \sigma} - \kappa h \phi = 0 \quad \text{on } \sigma = 0, \qquad \frac{\partial \phi}{\partial \sigma} = 0 \quad \text{on } \sigma = 1. \tag{9}$$

For a general eddy viscosity the eigenpairs $\{\phi_j(\sigma), \lambda_j\}$ depend on x and y and perhaps also on t. We assume the eigenfunctions are normalized in such a way that

$$\int_0^1 \phi_j(\sigma)^2 \, \mathrm{d}\sigma = 1. \tag{10}$$

Rather than expanding U directly, we obtain a more rapidly convergent series[7] if the function

$$V(\sigma) = \frac{S}{\kappa}\left(1 + \kappa h \int_0^\sigma \frac{\mathrm{d}\sigma'}{N(\sigma')}\right) \tag{11}$$

is first subtracted. Writing $U(\sigma) = V(\sigma) + W(\sigma)$, we obtain the following boundary value problem for W:

$$\frac{\partial W}{\partial t} + \mathrm{i}fW - h^{-2}\frac{\partial}{\partial \sigma}\left(N\frac{\partial W}{\partial \sigma}\right) = F, \tag{12}$$

$$\frac{\partial W}{\partial \sigma} = 0 \quad \text{on } \sigma = 1, \qquad N\frac{\partial W}{\partial \sigma} - \kappa h W = 0 \quad \text{on } \sigma = 0, \tag{13}$$

where

$$F = -g\left(\frac{\partial \zeta}{\partial x} + \mathrm{i}\frac{\partial \zeta}{\partial y}\right) - \frac{\partial V}{\partial t} - \mathrm{i}fV. \tag{14}$$

The essential point is that the boundary conditions (13) are now homogeneous. We now expand W in terms of the eigenfunctions:

$$W(\sigma)=\sum_j c_j \phi_j(\sigma). \tag{15}$$

In view of condition (10) and the usual orthogonality property of the eigenfunctions, the coefficients in the expansion (15) are given by

$$c_j=\int_0^1 W(\sigma)\phi_j(\sigma)\mathrm{d}\sigma. \tag{16}$$

Multiplying the differential equation (12) by $\phi_j(\sigma)$, integrating from $\sigma=0$ to $\sigma=1$ and using the boundary conditions (9) and (13), we obtain the following uncoupled system of differential equations for these modal amplitudes:[7]

$$\frac{\partial c_j}{\partial t}+(h^{-2}\lambda_j^2+\mathrm{i}f)c_j=R_{1j}(t)\left(\frac{\partial \zeta}{\partial x}+\mathrm{i}\frac{\partial \zeta}{\partial y}\right)+R_{2j}. \tag{17}$$

where

$$R_{1j}(t)=-g\int_0^1 \phi_j(\sigma)\mathrm{d}\sigma=-\frac{g\kappa h}{\lambda_j^2}\phi_j(0), \tag{18}$$

$$R_{2j}(t)=-\int_0^1 \frac{\partial V}{\partial t}\phi_j(\sigma)\mathrm{d}\sigma-\mathrm{i}f\int_0^1 V\phi_j(\sigma)\mathrm{d}\sigma. \tag{19}$$

In the case when the eddy viscosity and surface shear stress are independent of t, the second of these reduces to

$$R_{2j}(t)=-\frac{\mathrm{i}fSh}{\lambda_j^2}\phi_j(1). \tag{20}$$

In order to obtain initial conditions for the system (17), we assume the motion starts from some given velocity $U=U_0$ at $t=0$. Then at $t=0$, $W=U_0-V$, so the initial values of the coefficients are given by

$$c_j(0)=-\int_0^1 [U_0(\sigma)-V(\sigma)]\phi_j(\sigma)\mathrm{d}\sigma. \tag{21}$$

For an initial state of rest, i.e. $U=0$ at $t=0$, we find

$$c_j(0)=-\frac{Sh}{\lambda_j^2}\phi_j(1). \tag{22}$$

Before setting up the numerical scheme, we need the equation relating p and q to the coefficients c_j. From (2) we have

$$\begin{aligned} p+\mathrm{i}q&=h\int_0^1 [V(\sigma)+W(\sigma)]\mathrm{d}\sigma \\ &=\frac{Sh}{\kappa}\left(1+\kappa h\int_0^1 \frac{1-\sigma}{N(\sigma)}\mathrm{d}\sigma\right)+\kappa h^2\sum_j \frac{c_j}{\lambda_j^2}\phi_j(0). \end{aligned} \tag{23}$$

3. FINITE DIFFERENCE SCHEMES

3.1. Interior points

Figure 1 shows the distribution of grid points at which the variables ζ, u and v are computed for the five horizontal grids investigated by Arakawa and Lamb. As discussed in Section 1, only the grids A, B, C and E will be considered here. For the A-, B- and E-grids all the variables u, v, p, q and c_j are computed at the same points. For the C-grid scheme it is necessary to split equation (17) into two real equations, since the real and imaginary parts relate to different grid points, and we set

$$c_j = a_j + \mathrm{i}b_j, \qquad R_{2j} = R_{2j}^x + \mathrm{i}R_{2j}^y.$$

The spatial finite difference approximations to equations (1) and (17) appropriate for these four grids are as follows.

Scheme A

$$\frac{\partial \zeta}{\partial t} + \overline{(\delta_x p)}^x + \overline{(\delta_y q)}^y = 0, \tag{24}$$

$$\frac{\partial c_j}{\partial t} + \alpha_j c_j = R_{1j}[\overline{(\delta_x \zeta)}^x + \mathrm{i}\overline{(\delta_y \zeta)}^y] + R_{2j}. \tag{25}$$

Scheme B

$$\frac{\partial \zeta}{\partial t} + \overline{(\delta_x p)}^y + \overline{(\delta_y q)}^x = 0, \tag{26}$$

$$\frac{\partial c_j}{\partial t} + \alpha_j c_j = R_{1j}[\overline{(\delta_x \zeta)}^y + \mathrm{i}\overline{(\delta_y \zeta)}^x] + R_{2j}. \tag{27}$$

Scheme C

$$\frac{\partial \zeta}{\partial t} + \delta_x p + \delta_y q = 0, \tag{28}$$

$$\frac{\partial a_j}{\partial t} + k_j a_j - f\overline{b_j} = R_{1j}\delta_x \zeta + R_{2j}^x, \tag{29a}$$

$$\frac{\partial b_j}{\partial t} + k_j b_j + f\overline{a_j} = R_{1j}\delta_y \zeta + R_{2j}^y. \tag{29b}$$

Scheme E

$$\frac{\partial \zeta}{\partial t} + \delta_x p + \delta_y q = 0, \tag{30}$$

$$\frac{\partial c_j}{\partial t} + \alpha_j c_j = R_{1j}(\delta_x \zeta + \mathrm{i}\delta_y \zeta) + R_{2j}. \tag{31}$$

(It is worth noting that grid E can be regarded as two interlocking C-grids.)

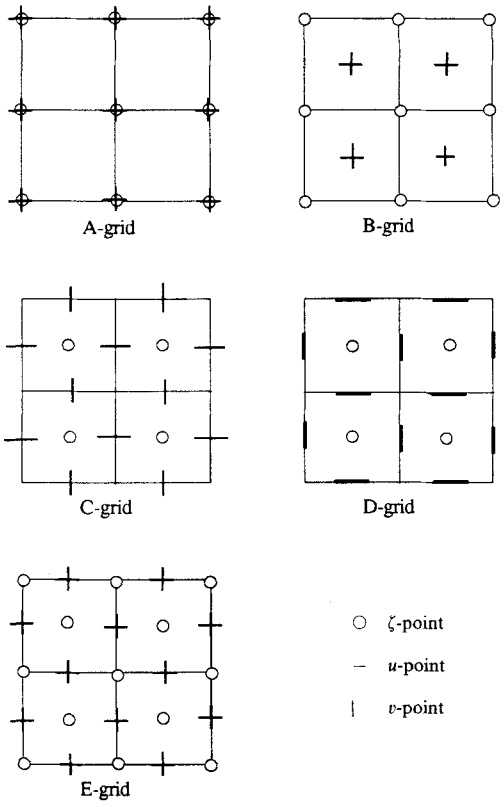

Figure 1. Arakawa grids A–E

In these equations the following notation is used for any net function β:

$$(\delta_x\beta)_{m,n}=\Delta x^{-1}(\beta_{m+1/2,n}-\beta_{m-1/2,n}), \qquad (\delta_y\beta)_{m,n}=\Delta y^{-1}(\beta_{m,n+1/2}-\beta_{m,n-1/2}),$$

$$(\bar{\beta}^x)_{m,n}=\tfrac{1}{2}(\beta_{m+1/2,n}+\beta_{m-1/2,n}), \qquad (\bar{\beta}^y)_{m,n}=\tfrac{1}{2}(\beta_{m,n+1/2}+\beta_{m,n-1/2}),$$

$$(\bar{\beta})_{m,n}=(\bar{\bar{\beta}}^{xy})_{m,n}=(\bar{\bar{\beta}}^{yx})_{m,n}.$$

Also, $k_j=h^{-2}\lambda_j^2$ and $\alpha_j=k_j+if$. It can be seen that the above schemes are all second-order in the spatial grid dimensions at points in the interior of the region. The treatment of boundary points in the various schemes will be discussed below.

The time-differencing scheme used for all four grids has been a leapfrog scheme in which ζ and c_j are computed at alternating half-steps, with equations (1) and (17) being used alternately to update each of these variables in turn.[7] This scheme has the advantage of being explicit and also second-order in the time step, though the size of the time step is restricted by the CFL stability criterion.

Since for the A-, B- and E-grids the two velocity components are taken at the same grid points, the differential equations for the c_j can be solved in complex form. Since this system is stiff, some care must be used in the choice of integration method. Writing equation (25), (27) or (31) in the

symbolic form

$$\frac{\partial c_j}{\partial t}+\alpha_j c_j=G_j, \tag{32}$$

we can update the solution over one time step from t to $t+\tau$ by the approximation[7]

$$\begin{aligned} c_j(t+\tau)&=c_j(t)\mathrm{e}^{-\alpha_j\tau}+\int_0^\tau G(t+s)\mathrm{e}^{-\alpha_j(\tau-s)}\mathrm{d}s \\ &\approx c_j(t)\mathrm{e}^{-\alpha_j\tau}+G(t+\tfrac{1}{2}\tau)r_j, \end{aligned} \tag{33}$$

where

$$r_j=\frac{1}{\alpha_j}(1-\mathrm{e}^{-\alpha_j\tau}).$$

The required value of G is found from ζ at the intermediate half-step, which has already been determined from the continuity equation.

For the C-grid the two real equations (29) must be integrated separately, but similar approximation formulae to (33) can be used, with α_j replaced by k_j and the Coriolis terms included with G. In order to have a stable treatment of the Coriolis terms, the two equations (29a) and (29b) are used in alternating order in successive time steps. This also has the advantage of providing a second-order scheme. A similar situation would occur also for the D-grid.

3.2. Treatment of boundary points

At a coastal boundary the boundary condition is taken to be that the normal component of volume flux, p or q, is equal to zero. As discussed in Section 1, it is not assumed that the normal velocity is zero throughout the water column. At an open boundary it is assumed for simplicity that the surface elevation ζ is prescribed. To illustrate how these boundaries are treated, examples of a left coastal boundary and a right open boundary are shown in Figures 2(a)–2(d) for the four numerical schemes respectively. Scheme C is of course well known but is included for completeness. It will be seen that in all the schemes the local truncation error is increased at the boundary points from second to first-order.

Scheme A: At point 1 in Figure 2(a) the boundary condition is $p=0$. In order to compute c_j from (25) at the adjacent interior point 2, it is necessary to know ζ at point 1. To compute this, (24) must be modified to have a one-sided difference in the x-direction; furthermore, q is required at the adjacent boundary points 3 and 4. These values can be found from (23), with c_j being computed from a modified version of (25) that uses a one-sided difference in the x-direction.

At the open boundary ζ is given at point 5. In order to compute ζ from (24) at the adjacent interior point 6, it is necessary to know p at point 5. This can be found from (23), with c_j being computed from a modified version of (25) that uses a one-sided difference in the x-direction.

Scheme B. At points 1 and 2 in Figure 2(b) the boundary condition is $p=0$. In order to compute ζ at the adjacent interior point 3, (26) must be modified to have a one-sided average of the q-term in the x-direction. In this scheme q is not computed at the boundary points 1 and 2, since use of (27) at these points would necessitate an extrapolation of ζ-values.

At the open boundary ζ is given at points 5 and 6 and c_j can be computed from (27) without modification at the adjacent interior point 7.

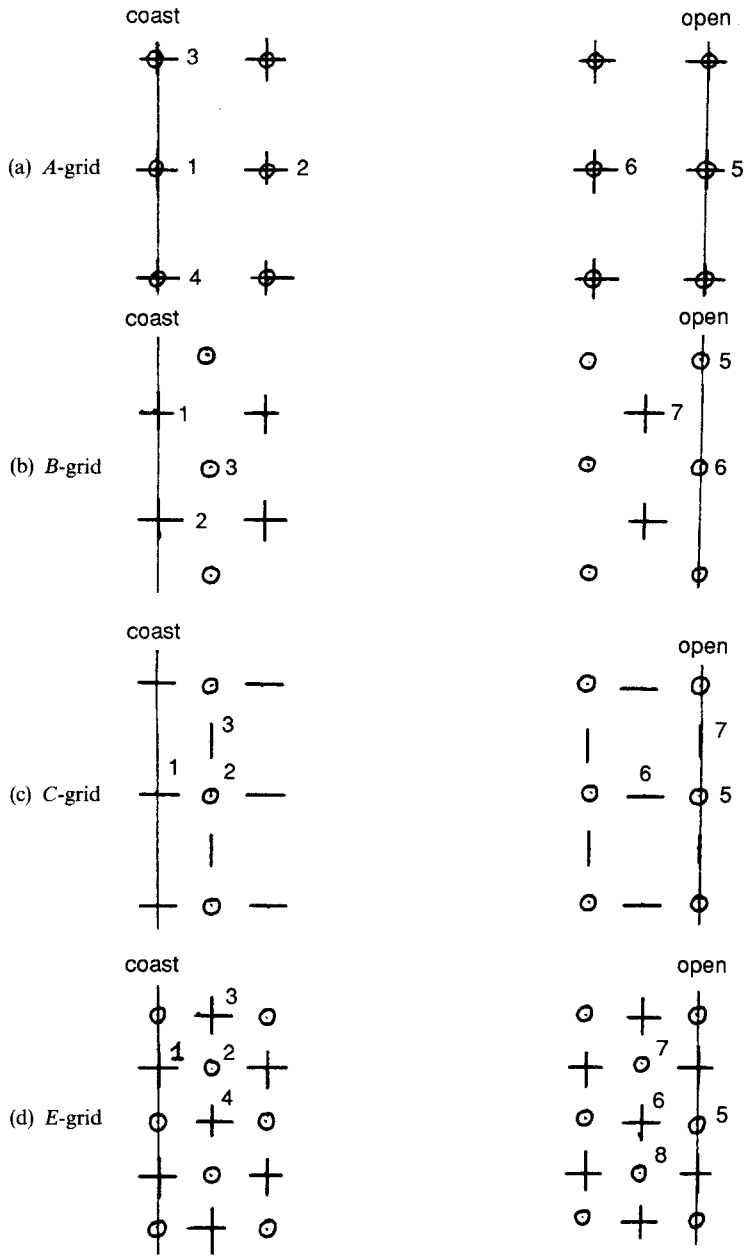

Figure 2. Treatment of coastal and open boundaries for A-, B-, C- and E-grids

Scheme C. At point 1 in Figure 2(c) the boundary condition is $p=0$ and ζ may be computed from (28) without modification at the adjacent interior point 2. The quantities a_j are not computed at the point 1. To compute b_j from (29b) at the interior point 3, all that is needed is to use Jamart and Ozer's wet-points-only averaging for the Coriolis term, i.e. to exclude points such as point 1 that lie on the boundary.

At the open boundary ζ is given at point 5. In order to compute a_j at the adjacent interior point, again (29a) is modified by including only interior points in the Coriolis term. The quantities b_j are not computed at points such as point 7 that lie on the boundary.

Scheme E. At point 1 in Figure 2(d) the boundary condition is $p=0$. In order to compute ζ from (30) at the adjacent interior point 2, it is necessary to know q at points 3 and 4. These can be found from (23), with c_j being computed at points 3 and 4 from a modified version of (31) that uses an extrapolated one-sided difference of ζ in the x-direction.

At the open boundary ζ is given at point 5. In order to compute c_j from (31) at the adjacent interior point 6, it is necessary to know ζ at points 7 and 8. This can be found from (30) with an extrapolated one-sided difference used for p in the x-direction. The use of extrapolated one-sided differences in this scheme is a potential weakness.

4. MODEL PROBLEMS

4.1. Closed rectangular sea

The four algorithms have been compared and tested using three model problems. The first of these is a simplified storm surge model of the North Sea used by Davies and Owen[3] and subsequently by several investigators to test algorithms. The model region consists of a closed rectangular sea of dimensions 400 km in the x-direction and 800 km in the y-direction, with grid spacings $\Delta x=400/9$ km and $\Delta y=800/17$ km. The depth is taken uniformly as 65 m. The sea is initially in a state of equilibrium and starting at $t=0$ is subjected to a constant surface shear stress in the negative y-direction with values $\tau_x=0$, $\tau_y=-1{\cdot}5\ \mathrm{N\,m^{-2}}$. The values of the other parameters (all in MKS units) are $\rho=1025$, $N=0{\cdot}065$, $\kappa=0{\cdot}002$, $g=9{\cdot}81$ and $f=1{\cdot}22\times10^{-4}$. A time step $\tau=360$ s was used.

Some typical computed results are shown in Table I, where typical velocity profiles after 30 h are tabulated for each of the four numerical schemes. The results are given for two grid points, one near the centre and one near the edge of the rectangle. An analytical solution is not known for this problem, so as a means of testing the accuracy of the numerical results, the same model problem has been recomputed using the B-grid scheme with grid spacings and time step equal to one-quarter of those stated above, and the results of this computation are listed in the first column of the table. Since the algorithms are all second-order at interior points and first-order at boundary points, it can be expected that the errors in the first column of the table are somewhere between one-quarter and one-sixteenth of the errors in the third column.

Comparing with the accurate numerical solution in the first column, we can see that Schemes B, C and E produce much more accurate results than scheme A. This is not surprising, in fact, since the approximations to the spatial derivatives in equations (24) and (25) involve finite differences over intervals of twice the size of those in the other three schemes. There appears to be little difference in accuracy among schemes B, C and E.

Secondly, none of the schemes generate spurious numerical boundary layers, presumably because for schemes A, B and E the momentum equations are solved at the same point and averaging is not needed for the Coriolis terms. For scheme-C such boundary layers do occur if the wet-points-only averaging is not employed.[6]

Thirdly, the CPU time required per time step of computation is about the same for schemes A, B and C but is approximately twice as much for scheme E. Again this is to be expected, since for the same grid spacing the E-grid has twice as many grid points as the other three grids, which all have about the same number of points.

Table I. Accurate and computed velocity profiles after 300 steps (30 h) for first test problem. Units are mm s^{-1}. Level 1 is at the bottom and level 10 is at the surface. The two tabulations refer to the C-grid points (2, 2) and (8, 10) respectively (The region is rectangular, running from (2, 2) to (10, 18).)

	Accurate solution		Scheme A		Scheme B		Scheme C		Scheme E	
Level	u	v	u	v	u	v	u	v	u	v
10	−97	−385	−129	−375	−98	−397	−97	−387	−94	−395
9	−83	−239	−116	−229	−84	−251	−83	−241	−80	−248
8	−48	−125	−81	−115	−49	−136	−48	−126	−45	−133
7	−5	−38	−38	−29	−6	−49	−5	−40	−2	−47
6	38	24	5	31	36	13	38	22	39	16
5	75	67	43	73	74	56	75	65	76	59
4	102	93	71	97	101	83	102	91	103	87
3	116	106	86	108	114	96	116	104	116	100
2	115	106	89	107	114	97	115	105	115	101
1	100	93	78	92	99	85	101	91	100	88
10	−144	−338	−148	−380	−148	−349	−145	−353	−144	−347
9	−130	−193	−134	−235	−134	−204	−131	−207	−130	−202
8	−94	−79	−98	−120	−98	−89	−95	−93	−94	−88
7	−50	5	−52	−35	−53	−4	−50	−8	−49	−3
6	−5	66	−7	26	−8	56	−5	52	−4	57
5	34	106	33	68	31	97	34	93	35	98
4	63	129	64	94	61	121	64	117	65	121
3	80	137	82	105	78	131	82	127	82	130
2	84	133	86	105	82	127	86	124	86	127
1	74	114	76	92	72	110	75	107	75	109

4.2. Open rectangular sea

The second model problem is one for which an analytical solution can be found. The region is again rectangular but with open boundaries on all sides on which the volume transports are specified as given below. The water depth is uniformly 65 m and the other parameters are given the same values as in the closed-sea problem except that κ is zero.

When the bottom friction is zero, the depth-integrated equations form a closed system. Integrating equations (3) from $z=-h$ to $z=0$ and using conditions (4) with $\kappa=0$, we get

$$\begin{aligned} \frac{\partial p}{\partial t}-fq &= -gh\frac{\partial \zeta}{\partial x}+s_x, \\ \frac{\partial q}{\partial t}+fp &= -gh\frac{\partial \zeta}{\partial y}+s_y, \end{aligned} \tag{34}$$

where $s_x=\tau_x/\rho$ and $s_y=\tau_y/\rho$. Equations (34) and (1) can be solved for p, q and ζ.

Analytical solutions can be found that depend on only one of the co-ordinates x and y. If $s_y=0$, a solution that starts from rest and is independent of y is given by

$$\zeta=s_x Z(x, t, l_x), \qquad p=s_x P(x, t, l_x), \qquad q=s_x Q(x, t, l_x),$$

where x runs from zero to l_x and

$$Z(x, t, l)=-l\sum_{n\,\text{odd}}\frac{4}{\omega_n^2}\left[1-\cos\left(\frac{\omega_n t}{l}\right)\right]\cos\left(\frac{n\pi x}{l}\right),$$

$$P(x, t, l) = l \sum_{n\,\text{odd}} \frac{4}{n\pi\omega_n} \sin\left(\frac{\omega_n t}{l}\right) \sin\left(\frac{n\pi x}{l}\right),$$

$$Q(x, t, l) = -fl^2 \sum_{n\,\text{odd}} \frac{4}{n\pi\omega_n^2} \left[1 - \cos\left(\frac{\omega_n t}{l}\right)\right] \sin\left(\frac{n\pi x}{l}\right),$$

with $\omega_n^2 = (fl)^2 + gh(n\pi)^2$. By superimposing two of these solutions, we get a solution of the form

$$\zeta(x, y, t) = s_x Z(x, t, l_x) + s_y Z(y, t, l_y),$$

$$p(x, y, t) = s_x P(x, t, l_x) - s_y Q(y, t, l_y),$$

$$q(x, y, t) = s_x Q(x, t, l_x) + s_y P(y, t, l_y).$$

This solution satisfies the boundary conditions

$$p = -s_y Q(y, t, l_y) \quad \text{on } x = 0 \text{ or } l_x,$$

$$q = s_x Q(x, t, l_x) \quad \text{on } y = 0 \text{ or } l_y.$$

When the bottom friction is zero, the Sturm–Liouville problem (8), (9) has a zero eigenvalue and the spectral amplitude of the corresponding (constant) eigenfunction is related to the depth-averaged solution discussed above. In the other modal equations (17) the coefficient $R_{1j} = 0$ and the amplitudes c_j can be found independently of the depth-integrated equations. When S and N are independent of t, the solution is given by[7]

$$c_j(t) = -\frac{hS\phi_j(1)}{\alpha_j \lambda_j^2} (if + k_j e^{-\alpha_j t}),$$

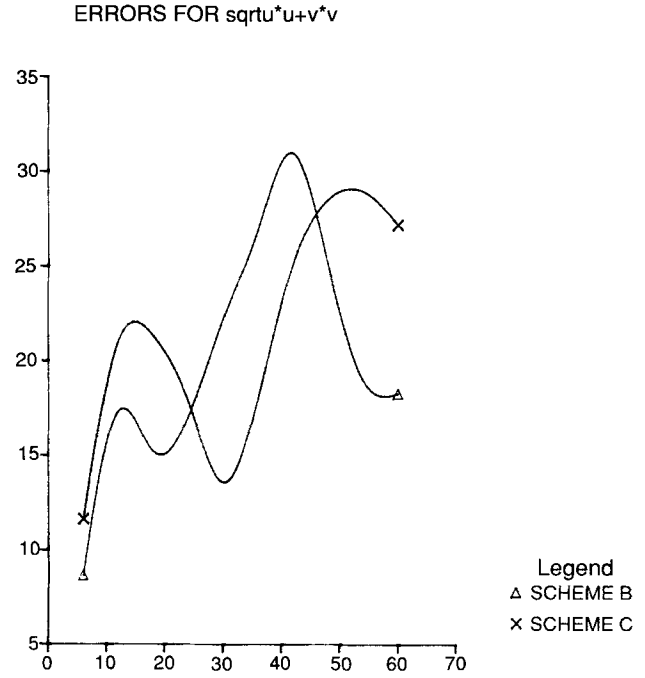

Figure 3. RMS errors in velocity as a function of time step for schemes B and C

where $k_j=h^{-2}\lambda_j^2$ and $\alpha_j=k_j+if$. In the special case when N is constant,

$$\phi_j(\sigma)=2^{1/2}\cos[j\pi(1-\sigma)], \qquad \lambda_j^2=N(j\pi)^2, \qquad k_j=N(j\pi/h)^2,$$

for $j\geqslant 1$, and the complete velocity field is given by

$$U(\sigma)=\frac{p+iq}{h}+\frac{hS}{2N}(\sigma^2-\tfrac{1}{3})-2hS\sum_{j\geqslant 1}\frac{\cos[j\pi(1-\sigma)]}{\alpha_j\lambda_j^2}(if+k_je^{-\alpha_j t}).$$

The numerical results obtained for this test problem lead to conclusions that are consistent with those from the first model problem. Scheme A is considerably less accurate than schemes B, C and E and in fact is sufficiently inaccurate to be unusable with the chosen grid sizes. The computational errors from schemes B, C and E are of comparable magnitudes, with the E-grid being slightly more accurate than the other two but also being roughly twice as computationally expensive.

Figure 3 shows the RMS (root mean square) error in u and v combined for the B- and C-grids for the first 600 steps. Up to about 240 time steps (24 h) the B-grid results are more accurate than those from the C-grid, between 240 and 450 steps the C-grid produces more accurate results and from 450 to 600 steps the B-grid again becomes the more accurate. Graphs of the maximum errors in u and v over all grid points and levels are given in Figure 4 and show similar behaviour to the RMS errors. Up to about 300 steps the maximum errors in both u and v are smaller for the B-grid than for the C-grid, then the C-grid becomes more accurate for a number of steps, but at 600 steps the B-grid again has smaller maximum errors in both components of velocity.

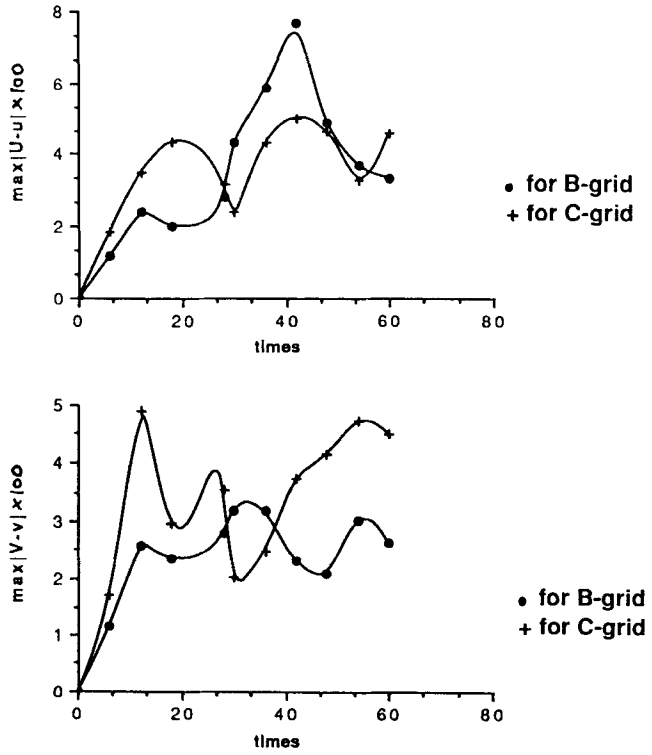

Figure 4. Maximum absolute errors in velocity as a function of time step

Table II. Exact and computed velocity profiles after 300 steps (30 h) for third test problem. Units are mm s^{-1}. Level 1 is at the bottom and level 10 is at the surface. The three tabulations refer to the B-grid points (2, 2), (7, 9) and (9, 6) respectively. (The region is irregular, consisting of a rectangle running from (1, 1) to (10, 12) minus two 3×3 squares in the upper left and lower right corners.)

	Accurate solution		Scheme B		Scheme C	
Level	u	v	u	v	u	v
10	−132	−381	−133	−381	−134	−373
7	−40	−36	−42	−37	−43	−29
4	69	91	66	89	66	96
1	77	87	75	86	74	91
10	−162	−391	−161	−393	−168	−401
7	−69	−46	−69	−47	−75	−56
4	46	83	43	80	37	72
1	62	82	59	80	56	75
10	−157	−394	−155	−388	−158	−392
7	−65	−49	−64	−43	−66	−46
4	48	79	46	83	44	80
1	63	80	61	81	60	79

4.3. Region with irregular boundaries

Finally, we have compared the accuracies of the B- and C-grid algorithms when the region has a boundary of irregular shape. The region consists of a rectangle of size 7×9 minus two squares of size 3×3 grids in the lower right and upper left corners of the rectangle. The other parameters and the wind stress are the same as in the first problem. As in the first problem, the control solution was computed using one of the algorithms with a much finer grid and smaller time step.

The velocity components after 300 steps at four levels and at three randomly scattered points within the region are given in Table II. It can be seen that the accuracies of the two algorithms are comparable, with the B-grid producing somewhat more accurate values at most of the chosen points and levels.

5. CONCLUSIONS

Algorithms have been developed for the numerical solution of the three-dimensional tidal equations using a spectral method in the vertical dimension and finite differences in the horizontal. Four difference schemes have been constructed based on the Arakawa A-, B-, C- and E-grids shown in Figure 1. While the C-grid has traditionally been used for such hydrodynamical computations, the other three grids offer significant advantages when a spectral method is used in the vertical, especially in that they allow eddy viscosity functions to be used that vary quite arbitrarily with position without introducing coupling among the modal equations.

A second advantage of these three grids is that none of them produces the spurious numerical boundary layers that can occur for the C-grid unless the Coriolis terms are treated using 'wet-points-only' averaging at coastal points.[6] A third benefit is that the two modal momentum equations can be solved simultaneously in complex form, allowing explicit numerical treatment of the Coriolis terms to be easily avoided (see equations (32) and (33)).

The four algorithms have been compared using three test problems. The conclusions reached are as follows.

The numerical errors arising for the A-grid were very significantly greater than those for the other three grids, the reason being, presumably, that the finite difference approximations to the various spatial derivatives must use intervals of twice the size.

The numerical errors for the E-grid were generally slightly lower than those for the C-grid for both test problems. The disadvantage of using the E-grid is that the computational cost is about twice that of the C-grid for the same grid dimensions. The computational costs of the B- and C-grids are about the same.

Both the RMS and maximum numerical errors in the velocity components for the B- and C-grids fluctuated in both relative and absolute magnitudes as the computations progressed. For the second problem, in which an analytical solution is known, over the first 600 time steps (60 h of real time) the B-grid results were on average slightly more accurate than those of the C-grid.

It is significant that the errors are almost uniform through the water column in every case, i.e. they are concentrated in the lowest mode. When the bottom friction is zero, as in the second test problem, the lowest mode is governed by the shallow water equations (1) and (34) in which there is no damping. It is therefore a pleasant surprise that the inferior numerical dispersion properties of the B- and E-grids at short wavelengths[15] do not lead to substantially greater errors in this problem than those for the C-grid. Both grids lead to stable algorithms for these undamped equations.

For a two-dimensional (depth-averaged) model the C-grid appears to have no disadvantages compared to the other grids. This would presumably also be true for a three-dimensional multilevel or splitting method. For spectral method algorithms, however, this grid imposes severe limitations on the physical model if the computation is to be easily feasible. Our results suggest that the B-grid can provide a viable alternative at the same computing cost and accuracy of solution without imposing such limitations.

Finally, it is worth noting that the spectral method with the Arakawa B-grid described in this paper has been extended to include the non-linear terms arising from advection and bottom friction[17] and has also been used to compute flow driven by density gradient.[18] Very accurate results have been obtained in test problems in both these extensions, and in an application of the second case, values were obtained that are consistent with earlier computations as well as with a rather limited amount of field data.

REFERENCES

1. N. S. Heaps, 'On the numerical solution of the three-dimensional hydrodynamical equations for tides and storm surges', *Mem. Soc. R. Sci. Liege, Ser.* **6**(2), 143–180 (1972).
2. N. S. Heaps, 'Three-dimensional model for tides and surges with vertical eddy viscosity prescribed in two layers I. Mathematical formulation', *Geophys. J. R. Astron. Soc.*, **64**, 291–302 (1981).
3. A. M. Davies and A. Owen, 'Three-dimensional numerical sea model using the Galerkin method with a polynomial basis set', *Appl. Math. Modell.*, **3**, 421–428 (1979).
4. A. M. Davies, 'Formulation of a linear three-dimensional hydrodynamic sea model using a Galerkin eigenfunction method', *Int. j. numer. methods fluids*, **3**, 33–60 (1983).
5. A. M. Davies, 'The numerical solution of the three-dimensional hydrodynamic equations using a B-spline representation of the vertical current profile', in J. C. J. Nihoul (ed.), *Bottom Turbulence, Proc. 8th Liege Conf on Ocean Hydrodynamics, Elsevier Oceanography Series, Vol. 19*, Elsevier, Amsterdam, 1977, pp. 1–25.
6. B. M. Jamart and J. Ozer, 'Numerical boundary layers and spurious residual flows', *J. Geophys. Res.*, **91**, 10.621–10.631 (1986).
7. R. W. Lardner, 'On the numerical solution of the linearized three-dimensional tidal equations using eddy-viscosity eigenfunctions', *J. Geophys. Res. C*, **95**, 22.269–22.274 (1990).
8. W. Hansen, 'Hydrodynamic methods applied to oceanographic problems', *Proc. Symp. on Mathematical–Hydrodynamical methods in Physical Oceanography*, Institut für Meereskunde, Universität Hamburg, 1962, pp. 24–34.

9. J. J. Leendertse, 'Aspects of a computational model for long period water-wave propagation', *Rand Corp. Tech. Rep. RM-5294-PR*, 1967.
10. R. T. Gedney and W. Lick, 'Wind-driven currents in Lake Erie', *J. Geophys. Res.*, **77**, 2714–2723 (1972).
11. B. Johns, P. C. Sinha, S. K. Dube, U. C. Mohanty and A. D. Rao, 'Simulation of storm surges using a three-dimensional numerical model: an application to the 1977 Andhra cyclone', *Q. J. R. Meteorol. Soc.*, **109**, 211–224 (1983).
12. J. O. Backhaus, 'A three-dimensional model for simulation of shelf–sea dynamics', *Dt. Hydrogr. Z.*, **38**, 165–187 (1985).
13. R. W. Lardner and H. M. Cekirge, 'A new algorithm for three-dimensional tidal and storm-surge computations', *Appl.Math. Modell.*, **12**, 471–481 (1988).
14. R. W. Lardner and P. Smoczynski, 'A vertical/horizontal splitting algorithm for three-dimensional tidal and storm-surge computations', *Proc. R. Soc. A*, **430**, 263–284 (1989).
15. A. Arakawa and V. R. Lamb, 'Computational design of the basic dynamical processes of the UCLA general circulation model', in *Methods in Computational Physics, Vol. 17*, Academic, New York, 1977, pp. 174–265.
16. J. R. Hunter, 'A note on quadratic friction in the presence of tides', *Estuar. Coastal Marine Sci.*, **3**, 473–475 (1975).
17. R. W. Lardner and Y. Song, 'A hybrid spectral method for the three-dimensional numerical modelling of nonlinear flows in shallow seas', *J. Computat. Phys.*, (1991) to be published.
18. Y. Song, S. K. Das and R. W. Lardner, 'Computation of densiy driven flows using the spectral method: application to the Arabian Gulf', *SFU Preprint*, 1991.